JOURNAL OF Materials CHEMISTRY

Refinement of thermodynamic data for $LaMnO_3$

K. T. Jacob* and Mrinalini Attaluri

Department of Metallurgy, Indian Institute of Science, Bangalore-560012, India. E-mail: katob@metalrg.iisc.ernet.in; Fax: +91-80-360 0683 or +91-80-360 0472; Tel: +91-80-394 2494

Received 2nd September 2002, Accepted 8th January 2003
First published as an Advance Article on the web 7th February 2003

The standard Gibbs energy of formation of $LaMnO_3$ has been measured in the temperature range from 900 to 1400 K using a solid-state cell incorporating a buffer electrode. The oxygen potential corresponding to the three-phase mixture MnO + La_2O_3 + $LaMnO_3$ has been measured using pure oxygen gas at 0.1 MPa as the reference electrode, and yttria-stabilized zirconia as the solid electrolyte. The buffer electrode prevented polarization of the three-phase electrode and ensured accurate data. The measured oxygen chemical potential corresponding to the decomposition of $LaMnO_{3-\delta}$ to MnO, La_2O_3 and O_2 gas is in fair agreement (± 6 kJ mol^{-1}) with most data available in the literature and can be represented by the equation,

$$\Delta\mu_{O_2}/\text{J mol}^{-1}\ (\pm 520) = -583160 + 170.55\ (T/\text{K})$$

Combining this with available information on oxygen potential variation with the non-stoichiometric parameter δ, the standard Gibbs free energy of formation of $LaMnO_3$ from MnO, La_2O_3 and O_2 was evaluated. The correction for non-stoichiometry was $\sim 1.6(\pm 0.7)$ kJ mol^{-1}. The heat capacity of $LaMnO_3$ has been measured by a differential scanning calorimeter from 400 to 1060 K. Information on low-temperature heat capacity available in the literature was joined smoothly with the high-temperature data to evaluate the standard entropy of $LaMnO_3$ at 298.15 K as 116.68 J mol^{-1} K^{-1}. The "third-law" analysis of the Gibbs energy values obtained in this study yields a value of -155.93 (± 0.8) kJ mol^{-1} for the standard enthalpy of formation of $LaMnO_3$ from MnO, La_2O_3 and O_2 at 298.15 K. This value provides a critical test of calorimetric data on enthalpy of formation of $LaMnO_3$. A consistent set of thermodynamic data for $LaMnO_3$ is presented from 298.15 to 1400 K based on the results obtained in this study and other supporting information in the literature.

1. Introduction

Doped lanthanum manganites, $La_{1-x}A_xMnO_3$ (A = alkaline earth element), with the perovskite structure exhibit giant magnetoresistance and find application in magnetic sensors and switches.[1–3] Because of the presence of oxygen vacancies, different oxidation states of manganese, and the consequent mixed electrical conductivity, doped $LaMnO_3$ can be used as electrodes for high-temperature fuel cells and as interconnection material in electrochemical reactors.[4–6] Lanthanum manganite is a good catalyst for the oxidation of carbon monoxide and ammonia and the reduction of oxides of nitrogen. In order to assess the compatibility of doped lanthanum manganites with support materials and solid electrolytes at high temperatures, accurate thermodynamic data are required. This article provides a critical review of thermodynamic data for pure $LaMnO_3$ reported in the literature and suggests refined values based on new measurements.

The low-temperature heat capacity of $LaMnO_3$ in the temperature range from 0.5 to10 K has been measured by Woodfield *et al.*[7] using semiadiabatic calorimetry. Satoh *et al.*[8] measured the heat capacity from 150 to 298 K by differential scanning calorimetry (DSC) and in the range 77 to 250 K using alternating current calorimetry (ACC). The combined results in the temperature range from 77 to 298 K are presented graphically and algebraically. The heat capacity data in two temperature intervals from 100 to 170 K and 665 to 764 K, corresponding to the two peaks, are also tabulated. Laberty *et al.*[9] used drop solution calorimetry with molten lead borate as solvent at 977 K to obtain a value of -74.8 (± 2.5) kJ mol^{-1} for the enthalpy of formation of $LaMnO_3$ at 298.15 K from its component binary oxides La_2O_3 and Mn_2O_3. From the calorimetric data they have computed the oxygen chemical potential for the dissociation of $LaMnO_3$ to La_2O_3, MnO and O_2 as a function of temperature.

Using thermogravimetry, Nakamura *et al.* (1273, 1473 K),[10] Kamata *et al.* (1473 K)[11] and Kitayama (1373 K)[12] studied the chemical stability of $LaMnO_3$ at controlled oxygen potentials generated by H_2 + CO_2 gas mixtures. Dissociation was indicated by a sudden mass change when the H_2–CO_2 ratio in the gas mixture was varied at constant temperature. From the results they calculated the Gibbs energy changes for the decomposition of $LaMnO_3$ to La_2O_3, MnO and O_2 gas. Borlera and Abbattista[13] have used gas chromatography to determine the equilibrium CO–CO_2 ratio corresponding to the decomposition of $LaMnO_3$ to La_2O_3, MnO and O_2 gas in the range 1173–1623 K. Vorobev *et al.*[14] measured the partial pressure of hydrogen in the gas phase in equilibrium with $LaMnO_3$, La_2O_3 and MnO under constant partial pressure of H_2O set by a thermostated cold trap in the temperature range from 1223 to 1323 K. By measuring the dependence of isothermal electrical conductivity on partial pressure of oxygen, Kamegashira *et al.*[15] have evaluated the Gibbs energy of formation of $LaMnO_3$ from MnO, La_2O_3 and O_2. Sreedharan *et al.*[16] and Atsumi *et al.*[17] used galvanic cells incorporating oxide solid electrolytes to measure the Gibbs energy of formation of $LaMnO_3$. $LaMnO_3$ in equilibrium with La_2O_3 and MnO is deficient in oxygen and can be represented as $LaMnO_{3-\delta}$. Except Kamata *et al.*,[11] all other investigators ignored the effect of non-stoichiometry of $LaMnO_{3-\delta}$ on its Gibbs energy.

Most of the measured oxygen potentials for the dissociation of $LaMnO_3$ at high temperatures,[10–15,17] except the values of Sreedharan *et al.*,[16] are in fair agreement (± 8.8 kJ mol^{-1}). However, the oxygen potentials computed from calorimetric

 DOI: 10.1039/b208550j

data are significantly more negative (for example, 72.8 kJ.mol^{-1} at 1100 K). New measurements were therefore conducted to resolve this discrepancy. The heat capacity of $LaMnO_3$ was measured using differential scanning calorimetry in the temperature range from 400 to 1060 K. The measured high-temperature heat capacity was then joined smoothly to low-temperature heat capacity reported in the literature to evaluate the entropy of $LaMnO_3$ as a function of temperature. The oxygen chemical potential corresponding to decomposition of $LaMnO_{3-\delta}$ was measured in the temperature range from 900 to 1400 K using an advanced version of the solid-state cell. The advanced features included the incorporation of a buffer electrode, which eliminated errors caused by electrode polarization, and a discontinuous noble metal barrier (Os) to prevent reaction between La_2O_3 at the electrode and the zirconia electrolyte. A small correction was applied for oxygen non-stoichiometry of $LaMnO_{3-\delta}$ samples in equilibrium with MnO and La_2O_3 to obtain Gibbs energy of formation of stoichiometric $LaMnO_3$. The "third-law" analysis was used to determine the enthalpy change for the decomposition reaction and the standard enthalpy of formation of $LaMnO_3$ at 298.15 K. A self-consistent set of thermodynamic properties of $LaMnO_3$ has been compiled from 298.15 to 1400 K.

2. Experimental methods

2.1. Materials

Lanthanum sesquioxide (La_2O_3) was heated at 1473 K for 3 h in high purity argon gas before use. Care was taken to prevent the formation of carbonates ($La_2O_2CO_3$) and hydroxides (LaOOH) by exposure of the oxide powder to ambient air. The sample for X-ray examination was mounted in petrolatum to prevent reabsorption of CO_2 and H_2O. La_2O_3 used in this study had the A-type structure (space group $P\bar{3}m1$), with a = 0.3938 nm and c = 0.6130 nm. The compound $LaMnO_3$ was prepared by solid-state reaction of La_2O_3 and Mn_2O_3, each of purity greater than 99.99%, at 1473 K for 2 days. Equimolar mixtures of oxide powders were compacted in a steel die before the heat treatment. Formation of single phase $LaMnO_3$ was confirmed by X-ray powder diffraction (XRPD). The lattice parameters of $LaMnO_3$ were determined by Rietveld refinement. The dimensions of the orthorhombic unit cell are a = 0.5745 nm, b = 0.7699 nm, c = 0.5536 nm. MnO was prepared by hydrogen reduction of Mn_2O_3 at 1073 K. The high purity argon gas, used to provide an inert cover for the alloys and electrodes, was first dried by passing through silica gel, anhydrous $Mg(ClO_4)_2$ and P_2O_5, and then deoxidized by passing through copper wool at 723 K and titanium granules at 1100 K.

2.2. High-temperature heat capacity measurements

A differential scanning calorimeter (DSC) was used to measure the heat capacity of $LaMnO_3$ under Ar gas from 400 to 1060 K. The sample was heat treated at 1273 K in Ar gas for 8 h before use. The oxygen non-stoichiometry of $LaMnO_3$ is negligible in high purity Ar gas. The average particle size of the powder sample was 6 μm. The DSC was operated in the step-heating mode to increase accuracy, with α-Al_2O_3 as the reference material. The alumina powder was dehydrated by vacuum treatment at 1200 K before use. The difference in heat flux into the sample and the reference material was integrated during heating at a constant rate (1 K min^{-1}) over small temperature steps (5 K) with an isothermal dwell time of 10 min. A λ-type transition with a heat capacity peak at 735 K was detected during preliminary studies. To evaluate the enthalpy corresponding to this higher order transition accurately, heat capacity was measured in the range 730–740 K in steps of 1 K. Analysis of $LaMnO_3$ by XRPD after the DSC experiment indicated no detectable change in its structure or lattice parameter.

2.3. Determination of phase relations in the system La–Mn–O

JCPDS-ICDD[18] lists several ternary oxides (La_2MnO_4, $La_2MnO_{4.15}$, $LaMnO_{3.15}$, $La_4Mn_4O_{11}$, $La_8Mn_8O_{23}$, and $LaMn_7O_{12}$) in the system La–Mn–O in addition to $LaMnO_3$. Design of solid-state cells for the determination of Gibbs energy of formation of ternary oxides requires a clear understanding of phase relations. Hence, phase relations in the system La–Mn–O at 1223 K were explored by equilibrating different mixtures of metals, alloys and oxides for ~6 days. Twice during the period, the samples were quenched, ground to –325 mesh, and repelletized for further heat treatment. Preliminary experiments indicated that ~4 days were sufficient to attain equilibrium. Samples representing 11 compositions used in this study are shown by an X in the ternary triangle displayed in Fig. 1. The samples containing metallic phases were equilibrated in closed molybdenum containers under pre-purified argon gas flowing at a rate of 200 ml min^{-1}. There was no interaction between the molybdenum container and La-rich alloys. There was some solid solubility of Mn in Mo for Mn-rich compositions. In such cases, the sample was supported on sacrificial pellets of the same composition. Oxide mixtures, containing manganese in the lower valence states, were equilibrated in closed zirconia crucibles, which were placed in evacuated quartz ampoules at a pressure of ~0.1 Pa. Oxide mixtures containing lanthanum and manganese in their highest oxidation states were equilibrated in pure dry oxygen at 0.1 MPa. There was negligible interaction between ZrO_2 crucible and the oxide phases at the experimental temperature.

After equilibration samples were quenched in liquid nitrogen or chilled mercury. Phase compositions of the quenched samples were determined using XRPD, SEM and EDS. To check for equilibrium, samples of the same overall composition were prepared using different starting materials. The approach to equilibrium from different directions was thus verified.

The oxygen content of the $LaMnO_{3+\delta}$ sample equilibrated in pure oxygen gas at 0.1 MPa pressure and 1223 K was determined by iodometry. The oxygen content of $LaMnO_{3-\delta}$ at its dissociation partial pressure at 1223 K was determined by thermogravimetry using CO–CO_2 gas mixtures, relative to the oxygen content of the sample in pure oxygen.

2.4. Measurement of Gibbs energies of formation of $LaMnO_3$

The reversible emf of the solid-state cell:

$$\text{Pt, MnO} + La_2O_3 + LaMnO_{3-\delta} \| (Y_2O_3)\ ZrO_2 \| O_2\ (0.1\ \text{MPa}), \text{Pt}$$

was measured as a function of temperature from 900 to 1400 K. The cell is written such that the right-hand electrode is positive.

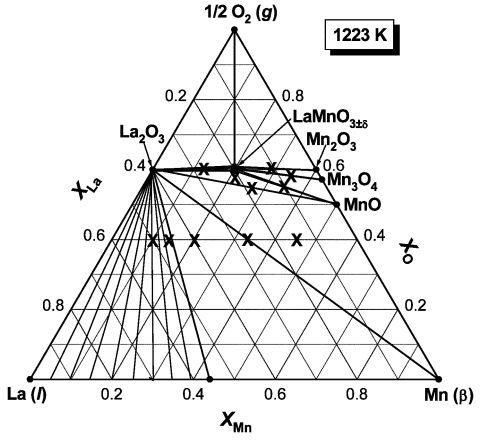

Fig. 1 Isothermal section of the ternary phase diagram for the system La–Mn–O at 1223 K.

The electrolyte (Y_2O_3) ZrO_2 is an oxygen ion conductor with ionic transport number greater than 0.99 at the temperatures and oxygen partial pressures encountered in this study.[19] However, the presence of trace electronic conduction in the electrolyte gives rise to a small electrochemical flux of oxygen from the reference electrode on the right side to the working electrodes on the left side of each cell.[20] The electrochemical permeability is caused by the coupled transport of oxygen ions and holes in the solid electrolyte under the oxygen potential gradient.

The electrochemical flux of oxygen would cause polarization of the multiphase solid electrodes. The chemical potential of oxygen in the microsystem near the solid-electrode–electrolyte interface would be altered because of the semi-permeability of the electrolyte to oxygen. A buffer electrode, introduced between reference and working electrodes was designed to act as a sink for the oxygen flux and prevent the flux from reaching the working electrode. The composition of the buffer electrode was the same as that of the working electrode at the start of the experiment. The small leakage current through the solid electrolyte membrane separating the reference and buffer electrodes was dissipated at the buffer electrode by an electrochemical reaction. The buffer electrode was maintained at an oxygen chemical potential close to that of the working electrode. Since there was no significant difference between the chemical potentials of buffer and working electrodes, driving force for transport of oxygen through the zirconia tube separating these electrodes did not exist. The working electrode therefore remained unpolarized. Pure oxygen gas at a pressure of 0.1 MPa, flowing over a platinized surface of zirconia, constituted the primary reference standard for oxygen potential and formed a non-polarizable electrode. Thus, the three-electrode design of the cell prevented error in emf caused by polarization of the working electrode. Measuring separately the emf between the three electrodes, two at a time, assessed the magnitude of the polarization effect. Transport of oxygen between the electrodes through the gas phase was prevented by physical isolation of the gas phase over the three electrodes.

The cell design used for high-temperature emf measurements is shown in Fig. 2. It consisted of three distinct compartments, separated by two impervious yttria-stabilized zirconia (YSZ) tubes closed at one end, a YSZ connecting tube and a YSZ crucible. An ionic bridge was provided through the buffer electrode. The cell can be represented schematically as follows:

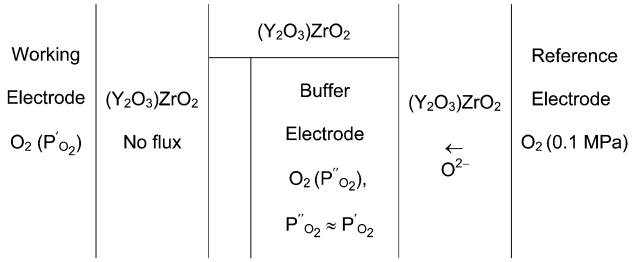

The working and reference electrodes were contained inside separate zirconia tubes. The cell emf measured between the working and reference electrodes was determined only by the oxygen chemical potential at these electrodes and not by the gradient of chemical potential through the connecting chain consisting of the solid electrolyte segments including the ionic bridge across the buffer electrode. Construction of the high-temperature galvanic cell was rendered more difficult by the introduction of the buffer electrode. The static sealed design used by Charette and Flengas[21] was found to be more appropriate than other designs that employ either dynamic vacuum or inert gas flow over the electrodes.[19,22]

The working electrode consisted of a mixture of La_2O_3 + $LaMnO_3$ + MnO in the molar ratio 1 : 1.5 : 1. An excess of the component that decomposed ($LaMnO_3$) to establish the oxygen pressure in the closed system was used. The average particle size of the powders used to prepare the working and buffer electrodes was in the range from 3 to 6 μm. The details of cell assembly and operational procedures used in this study were identical with those reported elsewhere.[23,24] At the end of each experiment, the electrodes were cooled to room temperature and examined by optical and scanning electron microscopy (SEM) and XRPD. Although small changes in the relative concentration of the constituents were observed in some cases, the number and nature of the phases remained unaltered. The change in relative concentration of the phases was consistent with the expected decomposition of $LaMnO_3$ at high temperature to generate the equilibrium oxygen pressures in sections of the apparatus.

Observed in preliminary experiments was a cyclic fluctuation in emf (± 2 mV) at constant temperature. At temperatures in excess of 1300 K, there was a gradual and unrecoverable drop of emf after a few hours of cell operation. The resistance of the cell increased with time, indicating the gradual formation of a non-conducting phase at the electrode–electrolyte interface. Careful examination of the interface using cross-sectional transmission electron microscopy (TEM) indicated islands of $La_2Zr_2O_7$. An attempt was made to prevent physical contact of La_2O_3 in the electrode with the solid electrolyte by inserting a thin Pt mesh. However, Pt–Mn alloy was formed during prolonged high-temperature exposure by partial decomposition of MnO at the low oxygen potential prevailing at the working electrode. Metallic Os was found to be relatively inert to MnO. Painted on all surfaces of the solid electrolyte in contact with the working and buffer electrodes was a solution of $OsCl_4$. After firing in air at 1275 K, a thin film of Os metal was obtained. The process was repeated three times to obtain a satisfactory coating on the whole contact surface. The Os film on the electrolyte converts partly into tiny spheres when held at 1375 K for 2 h. With the introduction of the spherical Os barrier at the electrode–electrolyte interface, the decay in emf was prevented.

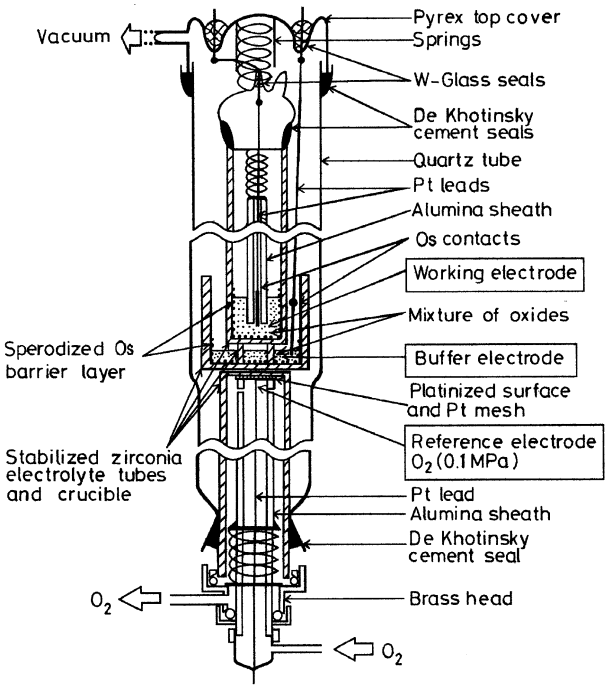

Fig. 2 Schematic diagram of the apparatus for high-temperature emf measurements; a buffer electrode is inserted between the reference and working electrodes to prevent polarization.

3. Results and discussion

3.1. Phase diagram for the system La-Mn-O

An isothermal section of the ternary phase diagram for the system La–Mn–O at 1223 K constructed from the results obtained in this study is shown in Fig. 1. Only one ternary compound $LaMnO_{3\pm\delta}$ was found to be stable. The La–Mn molar ratio in $LaMnO_{3\pm\delta}$ was $1(\pm 0.02)$. The oxygen content of $LaMnO_{3+\delta}$ in equilibrium with pure oxygen at 1223 K obtained by iodometric titration was 3.11. This value is in reasonable agreement with the recent results of Mizusaki *et al.*,[25] which show that δ decreases with increasing temperature from a value of 0.18 at 873 K to 0.10 at 1273 K. From structural considerations, interstitial oxygen defects are unlikely in perovskite-type compounds. The excess oxygen can be accounted for only in terms of vacancies on metal sites. If equal amounts of vacancies form on A and B sites, the defect structure can be written as $[La_{1-\alpha}V_\alpha][Mn_{1-\alpha}V_\alpha]O_3$ with $\alpha = \delta/3 + \delta$. However, if vacancies are selectively formed on the B-site and part of Mn enters the A-site, the compound can be represented as $[La_{1-\beta/2}Mn_{\beta/2}][Mn_{1-\beta}V_\beta]O_3$ with $\beta = 2\delta/3 + \delta$. Although, the latter scheme appears to be more probable since vacancy formation energies at the two sites are unlikely to be the same, more experimental evidence is required to differentiate between the models.

Along the binary La–O, La_2O_3 was the only stable oxide present. Along the binary Mn–O, the stable oxides MnO, Mn_3O_4 and Mn_2O_3 were identified. A liquid phase was stable for $0 \leqslant X_{Mn} \leqslant 0.44$ along the binary La–Mn. All the alloy phases were in equilibrium with La_2O_3. There was only one ternary oxide, $LaMnO_{3\pm\delta}$, which coexisted with La_2O_3 and all the oxides of manganese (MnO, Mn_3O_4 and Mn_2O_3) in different phase fields. A three-phase field involving $LaMnO_{3-\delta}$, La_2O_3 and MnO was identified. The measurement of the oxygen potential corresponding to this three-phase region permitted the evaluation of the standard Gibbs energy of formation of $LaMnO_{3-\delta}$. There was no ternary compound along the join La_2O_3–MnO.

At 1223 K, there was no evidence of phases with compositions La_2MnO_4, $La_2MnO_{4.15}$, $La_4Mn_4O_{11}$, $La_8Mn_8O_{23}$, and $LaMn_7O_{12}$ reported in the literature.[18] The phases $La_4Mn_4O_{11}$ ($LaMnO_{2.875}$), $La_8Mn_8O_{23}$ ($LaMnO_{2.75}$) form under reducing atmospheres from $LaMnO_3$ between 623 and 873 K.[26,27] They cannot be formed by the oxidation of La_2O_3 and MnO. They decompose into $LaMnO_3$, La_2O_3 and MnO when heated above 900 K. These observations suggest that composition $La_4Mn_4O_{11}$ and $La_8Mn_8O_{23}$ are metastable phases, produced by anion vacancy ordering during reduction of $LaMnO_3$. The compound $LaMn_7O_{12}$ is stable only at high-pressure.[28] The phase La_2MnO_4 prepared by the reduction of $La_{0.8}K_{0.2}MnO_3$,[29] probably had the composition $La_{2-X}K_XMnO_4$ and does not belong strictly to the ternary system La–Mn–O. The compound $La_2MnO_{4.15}$ is stable only above 1653 K.[13] The literature does not contain any information on phase relations in the system La–Mn–O for comparison with the results of this study.

3.2. Heat capacity and standard entropy of $LaMnO_3$

The heat capacity (C_p°) of $LaMnO_3$ in the temperature range from 400 to 1060 K at ambient pressure measured using DSC is plotted as a function of temperature in Fig. 3. A phase transition of order greater than one was observed at 735 K. The non-transition heat capacity ($C_{p,NT}^\circ$) of solid $LaMnO_3$ can be represented by the equation,

$$C_{p,NT}^\circ/\mathrm{J\ mol^{-1}\ K^{-1}} = 118.63 + 0.0286(T/\mathrm{K}) - 1922000\,(T/\mathrm{K})^{-2} - 49.4\,(T/\mathrm{K})^{-0.5} \quad (1)$$

The excess heat capacity ($C_{p,ex}^\circ$) corresponding to this transition was obtained by subtracting the baseline value (eqn. 1) from the measured values. The enthalpy and the entropy changes corresponding to the λ-type transition were determined as 3.46 kJ mol^{-1} and 4.9 J mol^{-1} K^{-1}, respectively, by evaluating $\int C_{p,ex}^\circ dT$ and $\int (C_{p,ex}^\circ/T) dT$ between the limits 565 K and 750 K. The data measured in this study is compared with values reported in the literature in Fig. 4. The high-temperature data obtained in this study closely agrees with that of Satoh *et al.*,[8] who also used a DSC and found a peak in heat capacity at 735 K. Their peak is narrower but slightly

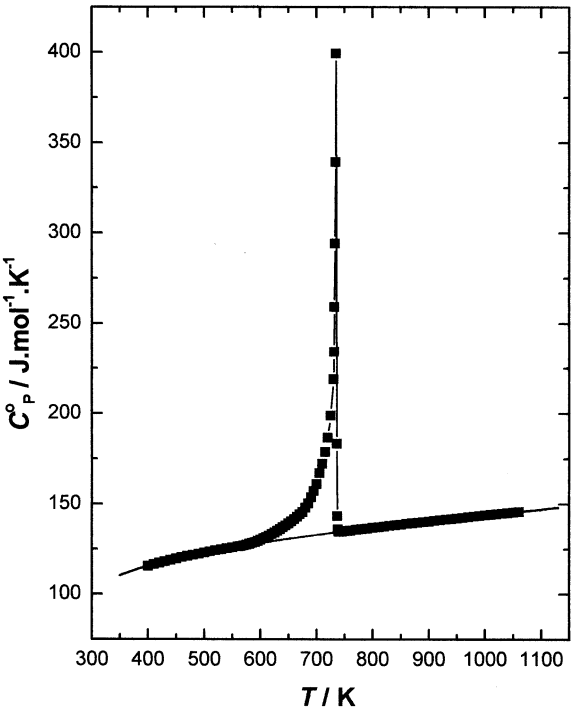

Fig. 3 Temperature dependence of the heat capacity of $LaMnO_3$ at ambient pressure measured in this study.

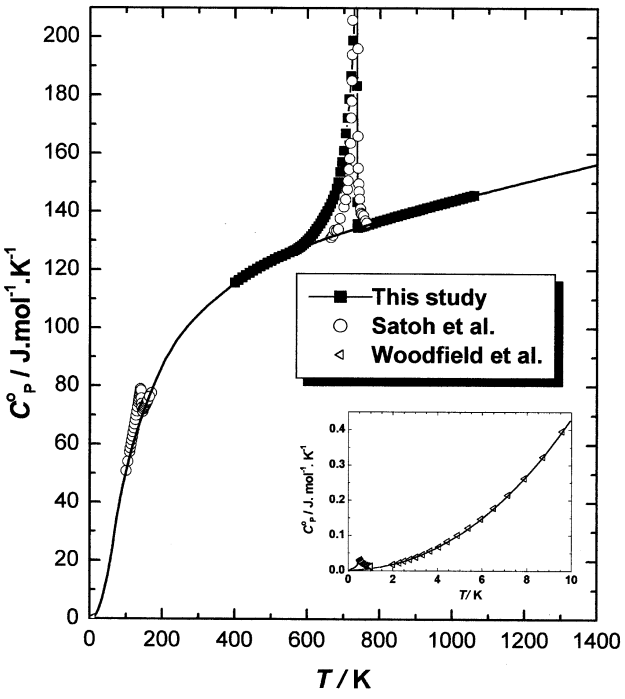

Fig. 4 Comparison of heat capacity data from different sources from 0 to 1400 K. The inset shows a magnified view of the low-temperature heat capacity data of Woodfield *et al.*[7] in the range from 0.5 to 10 K.

higher than that observed in this study. They have evaluated the enthalpy and the entropy change corresponding to the transition as 3.36 kJ mol^{-1} and 4.62 J mol^{-1} K^{-1} respectively, in good agreement with values obtained in this study.

The low-temperature heat capacity data measured by Woodfield *et al.*[7] in the range from 0.5 to 10 K and Satoh *et al.*[8] from 100 to 170 K are also displayed in Fig. 4. The low-temperature upturn below 1 K, shown in the inset, is caused by the large local magnetic field at the Mn nucleus because of electrons in unfilled shells and the consequent Mn-hyperfine contribution to the specific heat. The entropy change accompanying the hyperfine transition is 0.021 J mol^{-1} K^{-1}. Satoh *et al.* have reported a magnetic transition at 140 K, characterized by an enthalpy and entropy change of 220 J mol^{-1} and 1.7 J mol^{-1} K^{-1}, respectively. The low-temperature heat capacity data were smoothly merged with the high-temperature data obtained in this study as shown in Fig. 4. By integrating the low-temperature baseline heat capacity data and adding the entropy values for the two transitions, $S^{o}_{298.15K}$ ($LaMnO_3$) was evaluated as 116.68 ($\pm$1.5) J mol^{-1} K^{-1}.

3.3. Oxygen potential for three-phase equilibrium ($LaMnO_{3-\delta}$ + La_2O_3 + MnO)

Polarization of the buffer electrode was small but significant in the solid-state cell: the absolute value of the emf of the buffer electrode against the reference was 6 to 16 mV lower than that of the working electrode. The variation of the oxygen potential across the three-electrode cell is shown in Fig. 5. The polarization effect (E_p) is given by:

$$E_p = E_{r/w} - E_{r/b} - E_{b/w} \quad (2)$$

where, $E_{r/w}$ is the correct emf of the cell measured between the unpolarized reference and working electrodes, $E_{r/b}$ is the emf between the reference and buffer electrodes, and $E_{b/w}$ is the emf between the buffer and working electrodes. The emf across each solid electrolyte membrane is related to the oxygen potential difference across it. The polarization was more pronounced at high temperatures. Thus, the need for the buffer electrode for accurate thermodynamic measurements was clearly demonstrated.

The reversible emf of the cell is shown as a function of temperature in Fig. 6. The linear least-squares regression analysis of the emf gives,

$$E/\text{mV}\ (\pm 1.32) = 1511.0 - 0.4419\ (T/\text{K}) \quad (3)$$

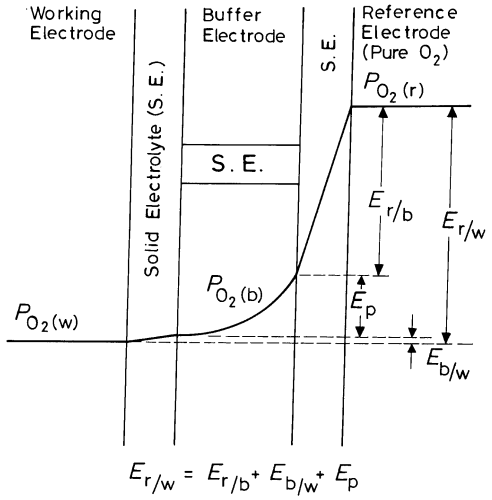

Fig. 5 Variation of the oxygen potential across the three-electrode cell assembly.

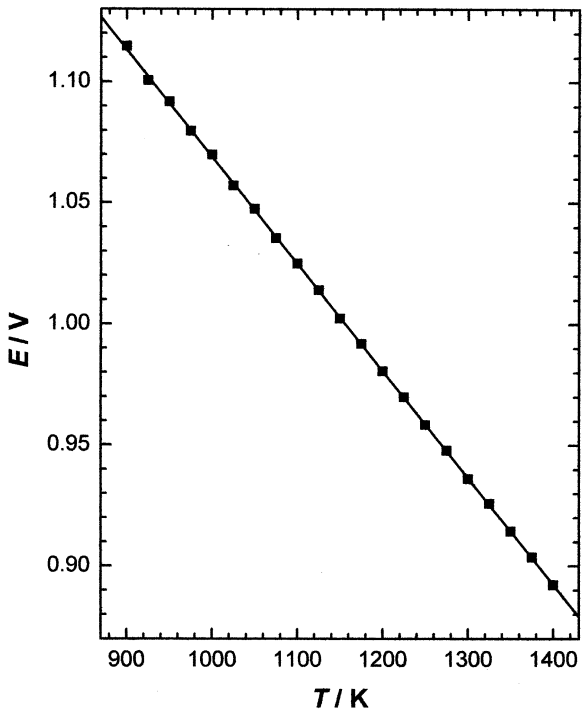

Fig. 6 Reversible emf of the cell as a function of temperature.

The emf of the cell is related to the oxygen potential of the three-phase equilibrium involving $LaMnO_{3-\delta}$, La_2O_3 and MnO defined by the reaction:

$$1/2\ La_2O_3 + MnO + (1-2\delta)/4O_2 \rightarrow LaMnO_{3-\delta} \quad (4)$$

$$\Delta\mu_{O_2}/\text{J mol}^{-1}\ (\pm 520) = -nFE = -583160 + 170.55(T/\text{K}) \quad (5)$$

In eqn. (5), F is the Faraday constant, $n = 4$ is the number of electrons involved in electrochemical reactions at each electrode, and $\Delta\mu_{O_2} = RT\ \ln P_{O_2}$ represents the relative chemical potential of oxygen. The uncertainty limit corresponds to twice the standard error estimate.

The oxygen potential defined by reaction (4) obtained in this study is compared in Fig. 7 with values reported in the literature. The differences between the values reported in literature and those obtained in this study are plotted as a function of temperature. The value reported by Nakamura *et al.*[10] using thermogravimetry at 1273 K is slightly lower, and their value at 1473 K is 5.6 kJ mol^{-1} higher than the results obtained in this study. Thermogravimetric measurements in H_2 + CO_2 gas by Kamata *et al.*[11] at 1473 K yield a value that is 3.39 kJ mol^{-1} higher. Using the same method, Kitayama[12] obtained values which are higher by ~6 kJ mol^{-1}. Borlera and Abbattista[13] used gas chromatography to determine the equilibrium CO–CO_2 ratio in the gas phase corresponding to the decomposition of $LaMnO_3$ to La_2O_3 and MnO in the range from 1173 to 1623 K. Their values are 1 to 2 kJ mol^{-1} more negative than those obtained in this study. The results of Vorobev *et al.*,[14] who have used gas–solid equilibrium technique in the temperature range from 1223 to 1323 K, show a different slope; but agree well with the results of this study at 1300 K. The values of Kamegashira *et al.*,[15] who used isothermal electrical conductivity to detect decomposition are higher by ~9 kJ mol^{-1}. Although simple to operate, it is difficult to ascertain multiphase equilibrium in the electrical conductivity method. The results of Sreedharan *et al.*,[16] obtained using a solid state cell standardized with respect to air as the reference, differ considerably both in magnitude (~18 kJ mol^{-1}) and slope

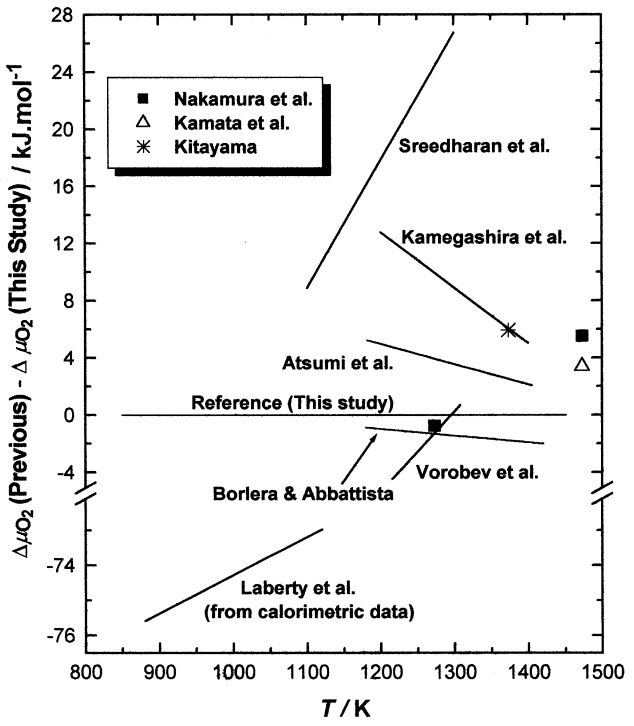

Fig. 7 Comparison of the oxygen chemical potential defined by the reaction 1/2 La_2O_3 + MnO + (1 − 2 δ)/4 $O_2 \rightarrow LaMnO_{3-\delta}$; the difference between the values reported by other investigators and that obtained in this study is plotted as a function of temperature.

from the values obtained in this study. The results of Atsumi *et al.*,[17] who used a solid state cell with Fe + Fe_XO as reference electrode are higher by 5.2 to 2.0 kJ mol^{-1}. Further, the value used by these authors for the chemical potential of oxygen at the reference electrode is ~500 J mol^{-1} more positive than that given in other evaluations.[30] If a correction were applied for the oxygen potential of their reference electrode, the results of their study would be a little closer to those obtained in this study. The values suggested by Laberty *et al.*,[9] based on their calorimetric measurements, are on an average 74.3 kJ mol^{-1} more negative than the values obtained in this study. The calorimetric data will be discussed in more detail in section 3.6 below.

3.4. Oxygen non-stoichiometry of $LaMnO_{3-\delta}$ at the phase boundary

"$LaMnO_3$" in equilibrium with La_2O_3 and MnO is deficient in oxygen, and can be represented as $LaMnO_{3-\delta}$. The value of δ as a function of partial pressure of oxygen has been reported by Kamata *et al.*[11] at 1473 K, Kuo *et al.*[31] from 1273 to 1473 K and Mizusaki *et al.*[25] from 873 to 1273 K. Borlera and Abbattista[13] have reported the limiting value of δ corresponding to the three-phase equilibrium in the temperature range from 1173 to 1723 K. The results of Borlera and Abbattista[13] show strong temperature dependence of δ at the phase boundary, varying form 0.015 at 1173 K to 0.095 at 1723 K. The other more recent studies[25,31] indicate only very mild or negligible temperature variation. Except for Kamata *et al.*[11] and Borlera and Abbattista,[13] others have presented the data only in a graphical form. Accurate values for the non-stoichiometric parameter at the phase boundary and its temperature dependence cannot be accurately assessed from the graphs. The results obtained in this study, which are in good agreement with those of Kamata *et al.*[11] and in fair agreement with those of Kuo *et al.*,[31] can be represented by the equation:

$$\ln \delta = -2.53 - 599.25/T\,(\mathrm{K}) \qquad (6)$$

3.5. Standard Gibbs energies of formation of $LaMnO_{3-\delta}$ and $LaMnO_3$

The standard Gibbs energy of formation of non-stoichiometric $LaMnO_{3-\delta}$ from La_2O_3, MnO and O_2 according to reaction (4) can now be computed:

$$\Delta_{r(4)}G^{\circ}/\mathrm{J\ mol^{-1}}\ (\pm 250) = \{(1-2\delta)/4\}\ RT \ln P_{O_2} = \{(1-2\delta)/4\}\ \Delta\mu_{O_2} = -137\,010 + 42.87(T/\mathrm{K}) \qquad (7)$$

where P_{O_2} is the equilibrium oxygen pressure obtained from the emf of the cell. It is useful to inquire if the Gibbs energy data for stoichiometric $LaMnO_3$ would be significantly different. To calculate the standard Gibbs energy of formation of $LaMnO_3$ (δ = 0) from the value for $LaMnO_{3-\delta}$, it is necessary to use Gibbs-Duhem integration. The compound $LaMnO_{3-\delta}$ may be considered as a phase with a constant ratio of mole fractions of La and Mn (X_{La}/X_{Mn}) and variable mole fraction of oxygen (X_O). The relative partial Gibbs energy of oxygen (ΔG_O = ½ $\Delta\mu_{O_2}$ = 0.5 $RT \ln P_{O_2}$) at any composition can be obtained from the variation of integral Gibbs energy of mixing (ΔG^M) with oxygen concentration using the basic equation[32]:

$$\Delta G_O = \Delta G^M + (1-X_O)\left(\frac{d\Delta G^M}{dX_O}\right)_{X_{La}/X_{Mn}} \qquad (8)$$

Dividing by $(1 - X_O)^2$,

$$\frac{\Delta G_O}{(1-X_O)^2} = \frac{\Delta G^M}{(1-X_O)^2} + \frac{1}{(1-X_O)}\left(\frac{d\Delta G^M}{dX_O}\right)_{X_{La}/X_{Mn}} = \frac{d}{dX_O}\left(\frac{\Delta G^M}{1-X_O}\right)_{X_{La}/X_{Mn}} \qquad (9)$$

By rearrangement one obtains,

$$d\left(\frac{\Delta G^M}{1-X_O}\right)_{X_{La}/X_{Mn}} = \frac{\Delta G_O}{(1-X_O)^2}dX_O \qquad (10)$$

Integrating along the path of constant X_{La}/X_{Mn},

$$\int_{X_O'}^{X_O''} d\frac{\Delta G^M}{(1-X_O)} = \int_{X_O'}^{X_O''} \frac{\Delta G_O}{(1-X_O)^2}dX_O \qquad (11)$$

Or,

$$(\Delta G^M)_{X_O''} = (\Delta G^M)_{X_O'}\left(\frac{1-X_O''}{1-X_O'}\right) + \left(1-X_O''\right)\int_{X_O'}^{X_O''} \frac{\Delta G_O}{(1-X_O)^2}dX_O \qquad (12)$$

The mole fraction of oxygen (X_O) is related to the non-stoichiometric parameter δ; $X_O = (3-\delta)/(5-\delta)$. The value of ΔG^M at any value of δ expressed in J.(gr.at.)$^{-1}$ is obtained by dividing $\Delta_f G^{\circ}$ for $LaMnO_{3-\delta}$ from elements by (5 − δ). The value of ΔG^M at the stochiometric composition (X_O'' = 0.6) at each temperature was obtained from the value for the nonstoichiometric phase-boundary composition (X_O'), using information in the literature[11,31] on the variation of chemical potential with nonstoichiometric parameter δ. From the value of ΔG^M at X_O'' = 0.6, the Gibbs energy of formation of stoichiometric $LaMnO_3$ according to the reaction,

$$1/2\ La_2O_3 + MnO + 1/4\ O_2 \rightarrow LaMnO_3 \qquad (13)$$

was computed at different temperatures. The results can be expressed by the equation:

$$\Delta_{r(13)}G^{\circ}/\mathrm{J\ mol^{-1}}\ (\pm 750) = -144\,290 + 42.68(T/\mathrm{K}) \qquad (14)$$

The uncertainty estimate includes errors in emf and temperature measurement as well as errors in the value of the non-stoichiometric parameter δ and its variation with oxygen partial pressure. If the oxygen non-stoichiometry was ignored and stoichiometric $LaMnO_3$ was assumed to be in equilibrium with La_2O_3 and MnO, the value for ($\Delta_{r(13)}G^o$/J mol^{-1}) would have been obtained as –145 790 + 42.64(T/K), with an uncertainty of ($\pm$130). Thus, the correction for non-stoichiometry is $\sim$1.6 kJ mol^{-1}. This correction for non-stoichiometry has not been applied by earlier investigators,[10,12–17] except Kamata *et al.*[11]

3.6. Standard enthalpy of formation of $LaMnO_3$

The values of Δ_rH^o (298.15 K) for reaction (13) can be evaluated from the high-temperature Gibbs energy values using the "third-law" method, which is based on the equation;

$$\Delta H^o(298.15) = \Delta G^o(T) - \int_{298.15}^{T} \Delta C_p^o \mathrm{d}T + T\{\Delta S^o(298.15) + \int_{298.15}^{T} (\Delta C_p^o/T)\mathrm{d}T\} \quad (15)$$

The "third-law" analysis is based on the knowledge of absolute entropies of reactants and products at 298.15 K. Furthermore, the high-temperature heat capacity of reactants and products should be available. These data for reactants were obtained from Pankratz,[33] while the high-temperature heat capacity and entropy of $LaMnO_3$ were taken from this study. The "third-law" analysis enables the calculation of the standard enthalpy change for the reaction at 298.15 K (Δ_rH^o (298.15 K)) from each value of Δ_rG^o at high temperature. When all the data are correct, the derived enthalpy change is independent of the temperature of measurement of Δ_rG^o. Drift of the derived enthalpy change at 298.15 K indicates error in at least one set of input data. The results of "third-law" analysis for reaction (13) are shown in Fig. 8. The scatter in the calcu- lated value of (Δ_rH^o (298.15 K)) is less than the uncertainty in Δ_rG^o. The average value for the standard enthalpy of reaction at 298.15 K is Δ_rH^o/kJ mol^{-1} = −155.93 with a drift of $\pm$0.3.

Laberty *et al.*[9] have reported a calorimetric value of −74.8 ($\pm$2.5) kJ mol^{-1} for the enthalpy of formation of $LaMnO_3$ at 298.15 K from its component oxides:

$$1/2\ La_2O_3 + 1/2\ Mn_2O_3 \rightarrow LaMnO_3 \quad (16)$$

This along with enthalpy of formation of Mn_2O_3 from MnO and O_2 as determined by the calorimetric measurements of Fritsch and Navrotsky[34] yields a value of −165.18 ($\pm$2.8) kJ mol^{-1} for reaction (13) which is 9.25 kJ mol^{-1} more negative than that obtained in this study. The value for $LaMnO_3$ reported by Laberty *et al.*,[9] when coupled with enthalpy of formation of Mn_2O_3 obtained from Pankratz,[33] yields a value of −169.07 kJ mol^{-1} for $\Delta_{r(13)}H^o$ (298.15 K) that is 13.14 kJ mol^{-1} more negative than that derived in this study. Thus, calorimetric data appears to suggest a more negative value for the enthalpy of formation of $LaMnO_3$ than that obtained from the Gibbs energy values.

To resolve this discrepancy, it is useful to look at calorimetric data on higher order systems. Laberty *et al.*[9] have also reported data on the enthalpy of formation of the solid solution $La_{1-X}Sr_XMnO_3$.The enthalpy changes for two different formation reactions at 298.15 K were measured as a function of the Sr content (X);

$$(1-X)/2\ La_2O_3\ (s) + X\ SrO(s) + 1/2\ Mn_2O_3(s) + X/4\ O_2(g) \rightarrow La_{1-X}Sr_XMnO_3(s) \quad (17)$$

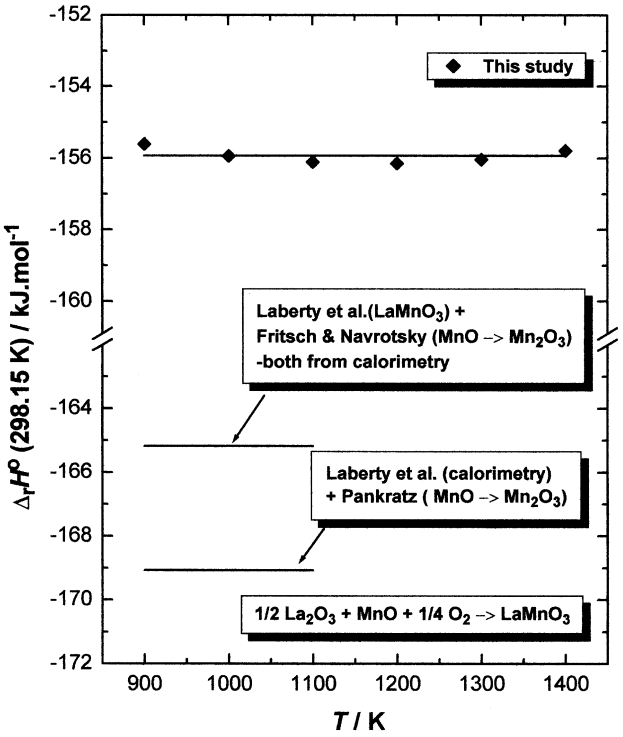

Fig. 8 Comparison of "third-law" analysis of high-temperature Gibbs energies of formation of $LaMnO_3$ obtained in this study with calorimetric data.

$$(1-X)/2\ La_2O_3\ (s) + X\ SrO(s) + (1-X)/2\ Mn_2O_3(s) + X\ MnO_2(g) \rightarrow La_{1-X}Sr_XMnO_3(s) \quad (18)$$

The measured data are shown as a function of X in Fig. 9. The enthalpy changes for both reactions vary linearly with Sr concentration (X) and extrapolate to the same value of

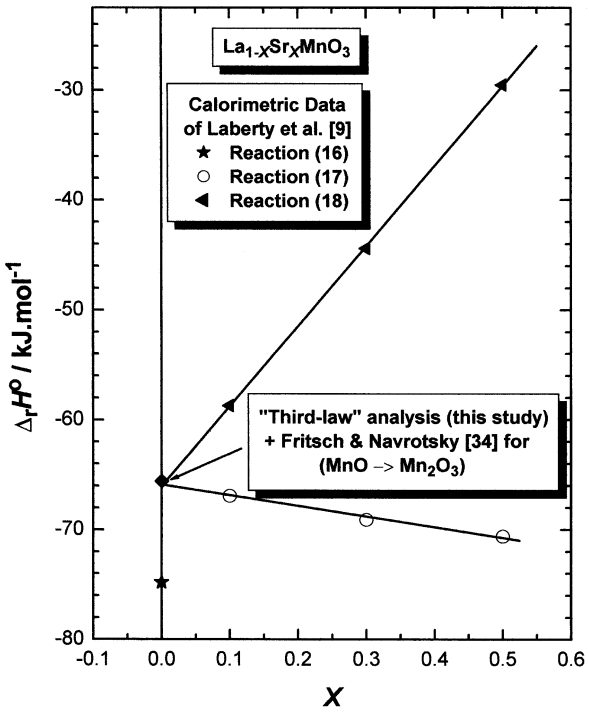

Fig. 9 Calorimetric data of Laberty *et al.*[9] for $La_{1-X}Sr_XMnO_3$ and $LaMnO_3$ compared with the results of "third-law" analysis. The data of Fritsch and Navrotsky[34] for the enthalpy of oxidation of MnO to Mn_2O_3 was used in conjunction with the "third-law" results for reaction (13) to obtain values for reaction (16).

Table 1 Recommended thermodynamic properties for $LaMnO_3$ from 298.15 to 1400 K

T/K	C_P^o/ J mol^{-1} K^{-1}	S^o/ J mol^{-1} K^{-1}	H_T^o–$H_{298.15}^o$/ kJ mol^{-1}	S_T^o–$S_{298.15}^o$/ J mol^{-1} K^{-1}	$((G_T^o$–$H_{298.15}^o)/T)$/ J mol^{-1} K^{-1}	$\Delta_f H^o$/ kJ mol^{-1}	$\Delta_f G^o$/ kJ mol^{-1}
298.15	102.65	116.68	0	0	−116.68	−1437.990	−1354.620
300	103.00	117.38	0.210	0.69	−116.68	−1437.970	−1354.060
400	115.59	148.97	11.200	32.29	−120.97	−1436.880	−1326.250
500	123.03	175.62	23.160	58.94	−129.30	−1435.180	−1298.770
600	128.43	198.55	35.740	81.86	−138.98	−1433.570	−1271.640
700	132.86	218.69	48.810	102.00	−148.96	−1431.490	−1244.820
706	133.11	219.82	49.610	103.14	−149.55	−1431.370	−1243.260
706	133.11	224.72	53.070	108.04	−149.55	−1427.910	−1243.260
800	136.76	241.59	65.760	124.90	−159.39	−1425.930	−1218.770
900	140.35	257.90	79.620	141.22	−169.43	−1423.840	−1193.010
1000	143.75	272.87	93.820	156.19	−179.05	−1423.960	−1167.410
1100	147.01	286.72	108.360	170.04	−188.21	−1421.860	−1141.820
1193	149.97	298.77	122.170	182.09	−196.36	−1423.190	−1118.110
1193	149.97	298.77	122.170	182.09	−196.36	−1429.390	−1118.110
1200	150.19	299.65	123.220	182.97	−196.96	−1429.220	−1116.260
1300	153.30	311.79	138.390	195.12	−205.34	−1426.730	−1090.320
1400	156.379	323.27	153.880	206.59	−213.36	−1426.290	−1064.440

−66.0 kJ mol^{-1} at $X = 0$, which corresponds to pure $LaMnO_3$. This extrapolated value is approximately 8.8 kJ mol^{-1} more positive than the value reported by the same authors[9] for pure $LaMnO_3$. Thus, the calorimetric data appear to be internally inconsistent. Further research is required to clarify the source of this discrepancy. The extrapolated value for enthalpy of formation agrees with the results obtained in the study within the combined uncertainty limits.

3.7. Consistent thermodynamic data for $LaMnO_3$ from 298.15 to 1400 K

A table of consistent thermodynamic data for $LaMnO_3$ can be developed from the evaluated information. The results are summarized in Table 1. The enthalpy of formation of $LaMnO_3$ from its elements La, Mn and O_2 at 298.15 K is obtained from the evaluated enthalpy change for reaction (13) and the enthalpies of formation of La_2O_3 and MnO from the compilation of Pankratz.[33] The standard entropy of $LaMnO_3$, evaluated from low-temperature heat capacity in section 3.2, is used as the cornerstone for entropy. Values for $\{H^o(T) - H^o(298.15)\}$, $S^o(T)$ and $\{S^o(T) - S^o(298.15)\}$ are evaluated from the high-temperature heat capacity measured in this study. The high-temperature λ-type transition is treated as an equivalent first order transition; the transition temperature is obtained by dividing the enthalpy of transition by the corresponding entropy, which are evaluated in section 3.2. The values of the Gibbs energy function,

$$((G^o_T - H^o_{298.15})/T) = -S^o_T + (H^o_T - H^o_{298.15})/T$$

are evaluated from the component terms. The entropy of formation of $LaMnO_3$ from the elements at each temperature is evaluated using the data assessed in this study for $LaMnO_3$ and values for La, Mn and O_2 from Pankratz.[33] Using the equation,

$$\Delta_f G^o = \Delta_f H^o - T\Delta_f S^o \quad (19)$$

values for the Gibbs free energy of formation of $LaMnO_3$ from elements are obtained at regular intervals of temperature. Current thermodynamic data compilations do not contain a complete set of data for $LaMnO_3$.

4. Conclusions

This article presents a method for precise measurement of the oxygen potential for three-phase equilibrium ($LaMnO_{3-\delta}$ + La_2O_3 + MnO) in the system La–Mn–O using a solid-state cell with a buffer electrode. The buffer electrode prevents polarization of the working electrode that is caused by the electrochemical transport of oxygen through the electrolyte. The buffer electrode absorbs the oxygen flux from the oxygen reference electrode and thus prevents it from disturbing the working electrode. The measured oxygen potentials are in fair agreement with earlier studies except those of Sreedharan *et al.*[16] However, values of oxygen potential computed from calorimetric data for the three-phase field involving $LaMnO_{3-\delta}$, La_2O_3 and MnO are found to be much too negative. Differential scanning calorimetry is used to measure the high temperature heat capacity of $LaMnO_3$ under Ar gas. The standard entropy of $LaMnO_3$ at 298.15 K is evaluated as 116.68 ($\pm$1.5) J mol K^{-1} from low-temperature heat capacity data, joined smoothly to high-temperature values. This information is coupled with the Gibbs energy of formation of $LaMnO_3$ and high-temperature heat capacity values to get a refined value for the enthalpy of formation of $LaMnO_3$ from La_2O_3, MnO and O_2 at 298.15 K: $\Delta_{r(13)}H^o_{298.15}$ ($LaMnO_3$)/ kJ mol^{-1} = −155.93 ($\pm$2). The derived heat of formation is compatible with calorimetric data on $La_{1-X}Sr_XMnO_3$ solid solution, but differs from the value for $LaMnO_3$ obtained using drop solution calorimetry. A consistent set of thermodynamic data for $LaMnO_3$ from 298.15 to 1400 K is presented in tabular form.

Acknowledgements

The authors are grateful to Professor Anthony Petric of McMaster University for helpful discussions.

References

1 K. Chahara, T. Ohno, M. Kasai and Y. Kozono, *Appl. Phys. Lett.*, 1993, **63**, 1990.
2 A. Urushibara, Y. Moritomo, T. Arima, A. Asamitsu, G. Kido and Y. Tokura, *Phys. Rev. B*, 1995, **51**, 14103.
3 R. Mahendran, R. Mahesh, N. Rangavittal, S. K. Tiwari, A. K. Raychaudhuri, T. V. Ramakrishnan and C. N. R. Rao, *Phys. Rev. B*, 1996, **53**, 3348.
4 J. A. M. van Roosmalen, E. H. P. Cordfunke, R. B. Helmholdt and H. V. Zandbergen, *J. Solid State Chem.*, 1994, **110**, 100.
5 J. A. M. van Roosmalen, J. P. P. Huijsmans and L. Plomp, *Solid State Ionics*, 1993, **66**, 279.
6 O. Yamomoto, Y. Takeda, R. Kanno and M. Noda, *Solid State Ionics*, 1987, **22**, 241.
7 F. Woodfield, M. L. Wilson and J. M. Byers, *Phy. Rev. Lett.*, 1997, **78**(16), 3201.
8 H. Satoh, M. Takagi, K. Kinukawa and N. Kamegashira, *Thermochim. Acta.*, 1997, **299**, 123.
9 C. Laberty, A. Navrotsky, P. Alphonse and C. N. R. Rao, *J. Solid State Chem.*, 1999, **145**, 77.

10 T. Nakamura, G. Petzow and L. J. Gauckler, *Mat. Res. Bull.*, 1979, **14**, 649.
11 K. Kamata, T. Nakajima, T. Hayashi and T. Nakamura, *Mat. Res. Bull.*, 1978, **13**, 49.
12 K. Kitayama, *J. Solid State Chem.*, 2000, **153**, 336.
13 M. L. Borlera and F. Abbattista, *J. Less Common Met.*, 1983, **92**, 55.
14 Yu. P. Vorobev, A. A. Novlev, S. A. Leontev, A. N. Men, S. A. Prokudina and Ya. S. Rubinchik, *Inorg. Mater.*, 1979, **15**, 1142.
15 N. Kamegashira, Y. Miyazaki and Y. Hiyoshi, *Mater. Lett.*, 1984, **2**, 194.
16 O. M. Sreedharan, R. Pankajavalli and J. B. Gnanamoorthy, *High. Temp. Sci.*, 1983, **16**, 251.
17 T. Atsumi, T. Ohgushi and N. Kamegashira, *J. Alloys. Compds.*, 1996, **238**, 35.
18 JCPDS-ICDD, Joint Committee on Powder Diffraction Standards, Newtown Square, PA, USA.
19 J. N. Pratt, *Metall. Trans. A.*, 1990, **21A**, 1223.
20 J. Fouletier, P. Fabry and M. Kleitz, *J. Electrochem. Soc.*, 1976, **123**, 204.
21 G. G. Charette and S. N. Flengas, *J. Electrochem. Soc.*, 1968, **115**, 796.
22 G. M. Kale and K. T. Jacob, *Metall. Trans. B.*, 1992, **23B**, 57.
23 K. T. Jacob, T. H. Okabe, T. Uda and Y. Waseda, *J. Phase Equilibria*, 1999, **20**, 553.
24 K. T. Jacob, T. H. Okabe, T. Uda and Y. Waseda, *Mater. Sci. Eng. B*, 1999, **64**, 44.
25 J. Mizusaki, N. Mori, H. Takai, Y. Yonemura, H. Minamiue, H. Tagawa, M. Dokiya, H. Inaba, K. Naraya, T. Sasamoto and T. Hashimoto, *Solid State Ionics*, 2000, **129**, 163.
26 F. Abbattista and M. L. Borlera, *Ceram. Int.*, 1981, **7**, 137.
27 J. C. Grenier, J. Darriet, M. Pouchard and P. Hagenmuller, *Mater. Res. Bull.*, 1976, **11**, 1219.
28 B. Bochu, J. Chenavas, J. C. Joubert and M. Marezio, *J. Solid State Chem.*, 1974, **11**, 88.
29 E. M. Vogel and D. W. Johnson, *Thermochim. Acta*, 1975, **12**, 49.
30 B. C. H. Steele, in *Electromotive Force Measurements in High Temperature Systems*, ed. C. B. Alcock, Institute of Mining and Metallurgy, London, 1968, p.3.
31 J. H. Kuo, H. U. Anderson and D. M. Sparlin, *J. Solid State Chem.*, 1989, **83**, 52.
32 L. S. Darken, *J. Am. Chem. Soc.*, 1950, **72**, 2909.
33 L. B. Pankratz, *Thermodynamic Properties of Elements and Oxides*, Bull. U. S. Bur. Mines 1982, **672**, 214–278.
34 S. Fritsch and A. Navrotsky, *J. Am. Ceram. Soc.*, 1996, **79**(7), 1761.